

Journal of Biomedical Optics

BiomedicalOptics.SPIEDigitalLibrary.org

Label-free nanoscale characterization of red blood cell structure and dynamics using single-shot transport of intensity equation

Praveen Kumar Poola
Renu John

SPIE.

Praveen Kumar Poola, Renu John, "Label-free nanoscale characterization of red blood cell structure and dynamics using single-shot transport of intensity equation," *J. Biomed. Opt.* **22**(10), 106001 (2017), doi: 10.1117/1.JBO.22.10.106001.

Label-free nanoscale characterization of red blood cell structure and dynamics using single-shot transport of intensity equation

Praveen Kumar Poola and Renu John*

Indian Institute of Technology Hyderabad, Department of Biomedical Engineering, Kandi, Telangana, India

Abstract. We report the results of characterization of red blood cell (RBC) structure and its dynamics with nanometric sensitivity using transport of intensity equation microscopy (TIEM). Conventional transport of intensity technique requires three intensity images and hence is not suitable for studying real-time dynamics of live biological samples. However, assuming the sample to be homogeneous, phase retrieval using transport of intensity equation has been demonstrated with single defocused measurement with x-rays. We adopt this technique for quantitative phase light microscopy of homogenous cells like RBCs. The main merits of this technique are its simplicity, cost-effectiveness, and ease of implementation on a conventional microscope. The phase information can be easily merged with regular bright-field and fluorescence images to provide multidimensional (three-dimensional spatial and temporal) information without any extra complexity in the setup. The phase measurement from the TIEM has been characterized using polymeric microbeads and the noise stability of the system has been analyzed. We explore the structure and real-time dynamics of RBCs and the subdomain membrane fluctuations using this technique. © 2017 Society of Photo-Optical Instrumentation Engineers (SPIE) [DOI: [10.1117/1.JBO.22.10.106001](https://doi.org/10.1117/1.JBO.22.10.106001)]

Keywords: quantitative phase microscopy; label-free imaging; real-time microscopy.

Paper 170252RR received Apr. 18, 2017; accepted for publication Aug. 23, 2017; published online Oct. 5, 2017.

1 Introduction

Most of the biological microscopy specimens, in particular live cells, are transparent and the absorbed or scattered visible light from the cell is low. In live cell imaging, it is hard to create an image of a cell that is transparent with a very small refractive index change with respect to the surrounding media. A number of techniques like Zernike phase contrast microscopy¹ and Nomarski differential interference contrast microscopy,² developed in the past for imaging transparent biological specimens without staining, play an important role in modern biology, medicine, and optical metrology.^{3,4} In spite of their enormous value as *in vitro* imaging tools, they lack subcellular specificity and are inherently qualitative. Fluorescence microscopy^{5,6} using intrinsic or extrinsic contrast agents is yet another popular technique that offers molecular specificity and high spatial resolution. However, the addition of extrinsic contrast agents or use of transgenics modify the cellular or molecular structures of the cell and are, therefore, not ideal for characterization of live cells in their native physiological state. Quantifying the optical phase shifts associated with biological structures provides important information because it allows determination of the optical thickness profile of transparent objects with subwavelength accuracy.^{7,8} Measurement of phase distribution can deliver the internal structure and dynamics of the structures within the cells in three-dimensions (3-D). Therefore, measuring the phase of the cells in real time, quantitatively and nondestructively, has a unique meaning and value in microscopy.^{9,10} Significant progress has been achieved in quantitative phase microscopy in the past two decades to overcome the limitations of traditional phase imaging,¹¹ through development of new

techniques such as Fourier phase microscopy,¹² Hilbert phase microscopy,¹³ diffraction phase microscopy,¹⁴ digital holographic microscopy,^{15–17} in-line holography,¹⁸ tomographic phase microscopy,¹⁹ spatial light interference microscopy,²⁰ wide-field digital interferometry,²¹ and spatial phase-shifting methods.²² In all these methods, the refractive index profile is reconstructed for a single wavelength of illumination. There have been quite a few successful attempts to measure the refractive index of human red blood cells (RBCs) at multiple wavelengths using spectroscopic phase microscopy,²³ spectroscopic diffraction phase microscopy,²⁴ quantitative dispersion microscopy,²⁵ quantitative phase spectroscopy,²⁶ and dynamic spectroscopic phase microscopy.²⁷ In some of these methods, a white-light source with red, green, and blue color filters or a diffraction grating has been used to filter the spectral components. Lasers with multiple wavelengths have been used as light sources and complex experimental setups using Mach–Zehnder interferometric systems have been employed.²⁸ All of the above techniques require complex computational efforts and a sensitive experimental setup.

Transport of intensity equations microscopy (TIEM), on the other hand, has a relatively simple experimental setup, is easily implementable with white light illumination, and is cost-effective.^{29–32} In general, transport of intensity equation (TIE) requires one in-focus and two defocused images to be registered along the optical axis^{29–32} for reconstruction of phase images. However, when the phase of an object becomes a time-dependent signal, or when we need to observe dynamic events, we need to record the three images instantaneously. A number of techniques have been proposed for simultaneous recording of

*Address all correspondence to: Renu John, E-mail: renujohn@iith.ac.in

different defocused images in the past. One of the approaches utilizes chromatic dispersion³³ of a lens with white light illumination to get dispersion and uses this lens aberration to record three images at a time using a color camera. This technique is interesting, however, it has been reported that the pixel misregistration among the RGB components could create phase artifacts. Also, the defocus distance from these chromatic dispersions is limited within the visible spectra affecting the accuracy of phase for thicker biological samples like RBCs. Another interesting way of collecting focal image stacks was reported using fluidics,³⁴ wherein the transport of cells in a microfluidic device through the focal plane of a microscope has been exploited. Along the same lines, with minimal changes in bright-field microscope hardware, a single-shot TIE setup has been reported,³⁵ which utilizes a multiplexed volume hologram to laterally separate the images from different focal planes. The crosstalk between the multiplexed gratings might result in noise artifacts in the reconstructed images. Other techniques to instantaneously record multiple images in TIE were reported using a beam splitter,³⁶ an electrical tunable lens,³⁷ and by displaying a set of lenses with different focal powers on a spatial light modulator.³⁸

Paganin et al.³⁹ demonstrated the principle of TIE for simultaneous phase and amplitude extraction from a single defocused image with homogeneity assumption on latex beads using x-rays. In this paper, we adapt the above single-shot TIE algorithm to visible light for imaging of homogeneous samples like RBCs since the principle behind the TIE equations are quite general and can be applied to any linear shift invariant system.⁴⁰ Earlier reports in this field have generalized the use of TIE in matter and radiational fields like Lorentz electron microscopy, diffraction enhanced imaging, neutron phase contrast imaging, and Nomarski microscopy with visible light.⁴¹ This technique requires only a partially coherent light source³² and is devoid of any speckles that are otherwise present in interferometric measurements. Biological cells, such as RBCs that are typically enucleated, can be considered to be homogenous.^{42–44} The assumption of homogeneity with an average refractive index of the cell makes the image reconstruction process simple and it can be operated in real time. We report high throughput and real-time analysis of RBC dynamics with the TIE technique through the recording of single defocused images of RBCs using a commercial bright-field microscope. We expect that it is possible to carry out fast screening of enucleated cells like RBCs in a very cost-effective manner under a regular bright-field microscope. In particular, this technique would be ideal for quantifying nanoscale structures and fluctuations of optically homogeneous cells like RBCs.

2 Principle

Phase objects can be rendered visible by slightly defocusing an optical microscope with white light illumination. It is known that the image contrast from a defocused image is proportional to the two-dimensional (2-D) Laplacian of the phase difference introduced by the phase object.^{45–47} Through defocused imaging, we study the wavefront curvature resulting from the surface modulations of the cell using the TIE principle. A detailed theory of phase retrieval from a single defocused image has been described by Paganin et al.³⁹ In this paper, we apply this technique based on a single defocused image to bright-field microscopy for studying the structure and dynamics of RBCs. The principle is outlined below [Eqs. (1)–(9)]. We assume that a

collimated plane beam of light of unit magnification is illuminating the sample.

Knowing the absorption coefficient μ of the sample for a particular wavelength (550 nm) band of illumination, the thickness of the sample t can be derived directly from the Lambert–Beer’s law

$$I(r_{\perp}, z = 0) = I^{\text{in}} e^{-\mu t(r_{\perp}, z)}, \quad (1)$$

where $t(r_{\perp})$ is the projected thickness of the homogeneous object onto the plane over which the image is taken, and I^{in} is the uniform intensity of the incident light.

If the object is sufficiently thin, the phase $\varphi(r_{\perp}, z = 0)$ of the illuminating beam at the exit surface of the homogeneous object is proportional to the projected thickness given by

$$\varphi(r_{\perp}, z = 0) = -\frac{2\pi}{\lambda} \Delta n t(r_{\perp}, z), \quad (2)$$

where Δn is the difference between an object’s refractive index and its surrounding media.

The intensity evolution of a paraxial monochromatic scalar electromagnetic wave on propagation along the axial direction can be described by the transport of intensity equation as follows:

$$\nabla_{\perp} \cdot [I(r_{\perp}, z) \nabla_{\perp} \varphi(r_{\perp}, z)] = -\frac{2\pi}{\lambda} \frac{\partial I(r_{\perp}, z)}{\partial z}, \quad (3)$$

where $I(r_{\perp}, z)$ and $\varphi(r_{\perp}, z)$ are the intensity and phase of the beam, respectively, λ is the wavelength of light, r_{\perp}, z denotes the position vector (x, y) , which lies in the plane perpendicular to the optical axis z , and ∇_{\perp} is the gradient operator in the plane containing the position vector.

Substituting Eqs. (1) and (2) into Eq. (3), the resulting equation is nonlinear in $t(r_{\perp}, z)$ and may be rewritten as an equation linear in $e^{-\mu t(r_{\perp}, z)}$ by using the identity in Eq. (5), the proof of which is added in the [Appendix](#) for interested readers

$$-\frac{\Delta n}{\mu} I^{\text{in}} \nabla_{\perp}^2 e^{-\mu t(r_{\perp}, z)} = \frac{\partial I(r_{\perp}, z)}{\partial z}, \quad (4)$$

$$\Delta n \nabla_{\perp} \cdot [e^{-\mu t(r_{\perp}, z)} \nabla_{\perp} t(r_{\perp}, z)] = -\frac{\Delta n}{\mu} \nabla_{\perp}^2 e^{-\mu t(r_{\perp}, z)}. \quad (5)$$

Estimating the right-hand side of Eq. (4) using intensity measurements over two sufficiently closely spaced planes separated by a distance R_2

$$\frac{\partial I(r_{\perp}, z)}{\partial z} \approx \frac{I(r_{\perp}, z = R_2) - e^{-\mu t(r_{\perp}, z)} I^{\text{in}}}{R_2}. \quad (6)$$

Substituting Eq. (6) into Eq. (4) and rearranging, we get

$$\left(-\frac{R_2 \Delta n}{\mu} \nabla_{\perp}^2 + 1 \right) e^{-\mu t(r_{\perp}, z)} = \frac{I(r_{\perp}, z = R_2)}{I^{\text{in}}}. \quad (7)$$

Fourier transforming Eq. (7) gives

$$\mathfrak{F} \left[e^{-\mu t(r_{\perp}, z)} \right] = \mu \frac{\mathfrak{F} [I(r_{\perp}, z = R_2)] / I^{\text{in}}}{R_2 \Delta n |k_{\perp}|^2 + \mu}, \quad (8)$$

where k_{\perp} represents the spatial frequency coordinates, R_2 is the defocus distance, and I^{in} is the initial intensity that is considered to be uniform.

Taking the inverse Fourier transform of Eq. (8) and solving for thickness, we get

$$t(r_{\perp}, z) = -\frac{1}{\mu} \log_e \left(\mathfrak{F}^{-1} \left\{ \mu \frac{\mathfrak{F}[I(r_{\perp}, z = R_2)]/I^{\text{in}}}{R_2 \Delta n |k_{\perp}|^2 + \mu} \right\} \right). \quad (9)$$

Equation (9) gives the projected thickness $t(r_{\perp})$ of a homogeneous sample by solving TIE. The numerical implementation of Eq. (9) is realized by making use of fast Fourier transforms³⁹ and can yield rapid deterministic phase information from a single defocused image of the homogeneous object under study. Equation (9) is valid for a collimated plane beam illumination.

3 Experiments

Bright-field imaging is carried out on a regular inverted bright-field microscope (Carl Zeiss Axio-observer™), represented in the schematic diagram (Fig. 1). We have used homogeneous melamine resin 1- μm -sized microbeads (Sigma-Aldrich) with a known refractive index of 1.68, which were suspended in distilled water ($n_{\text{med}} = 1.33$) with a linear attenuation coefficient of $0.843 \mu\text{m}^{-1}$ for phase characterization of the system. Then RBCs are imaged using a tungsten halogen light source for bright-field imaging at a defocus distance of $15 \mu\text{m}$ using a CCD camera (1040×1388 pixels, pixel size: $6.45 \mu\text{m}$). An aberration-corrected microscope objective ($50\times$, 0.55 NA) is used for imaging the RBC dynamics in bright-field mode. A single defocused bright-field image is recorded and the

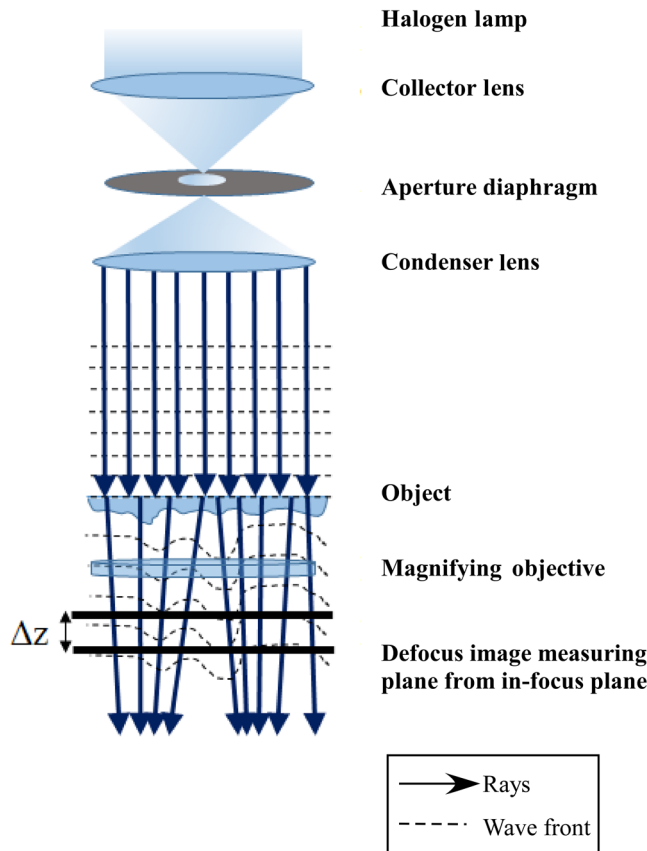


Fig. 1 Schematic of the experimental setup for TIE Imaging.

thickness of the RBC samples is computed on a MATLAB™ platform with the help of Fourier transforms using Eq. (9). RBCs were prepared for imaging according to standard protocols.⁴⁸ The cells were suspended in isotonic phosphate buffer solution with a refractive index of 1.334. Ten μl of RBCs were pipetted on to the glass slide and covered with a cover slip. We assume a linear attenuation coefficient (μ) of $0.2 \mu\text{m}^{-1}$ for the RBC at a wavelength of 550 nm (Ref. 49) and a refractive index of ~ 1.41 in the visible wavelength region.⁵⁰

4 Results and Discussions

We chose to first characterize the system using polymeric microbeads of known size to test the retrieved phase and for further validations. The defocused intensity recording [Fig. 2(a)] of polymeric microbeads was used to retrieve the 3-D phase using the TIE principle. Figure 2(b) shows the reconstructed 3-D phase image of the microbeads. A zoom-in depth view of the region marked in Fig. 2(b) (white square marked) is shown in Fig. 2(c). Figure 2(d) shows the retrieved profile of the thickness information. The microbeads are found to have an average size of $1 \pm 0.1 \mu\text{m}$, which is in agreement with the known microbead size.

We also characterize the spatial and temporal noise of the system by analyzing the phase noise.

In order to measure the phase noise of our system, we have used the following protocol that was previously reported.^{12–14,21} We recorded a video of defocused images for 600 s with a defocus distance of $1 \mu\text{m}$ and an exposure time of 19.6 ms using $50\times$ magnification (0.55 NA). Then we considered a spatial area of 50×50 pixels in the reconstructed image where there are no cells [red square marked in Fig. 2(b)]. After extracting each image frame from the video and reconstructing the phase images, the mean temporal standard deviation (SD) of thickness from frame to frame was found to be 0.02 nm [Fig. 2(e)] and the histogram of mean SD of the background spatial thickness was found to be 0.2 nm [Fig. 2(f)]. The above results show that the system shows a high phase sensitivity that is comparable to the previously demonstrated systems.^{12–14}

We have carried out experiments with RBCs after characterizing the system. The defocused intensity recordings [Fig. 3(a)] are used to retrieve the 3-D phase of RBCs using the TIE principle. Figure 3(b) shows the reconstructed 3-D phase image of the RBCs. A zoom-in depth view of the region marked in Fig. 3(b) is shown in Fig. 3(c). Figure 3(d) shows the retrieved volume of the sample in 3-D from the thickness information in Fig. 3(b). We have taken measurements from 15 RBCs for calculating the average height, volume, and diameter. The studies from our samples are found to have an average diameter of 6 to $8 \mu\text{m}$, which is comparable to the reported literature.^{51,52} The calculated average volumes of the RBCs were $65 \mu\text{m}^3$, as shown in Fig. 3(d). All these parameters are comparable and within the known ranges reported in the literature.^{51,52} The quantitative phase of the RBC rendered across the cell along the line marked on Fig. 4(a) is depicted in Fig. 4(b). The results from this technique accurately show the characteristic thickness profile of an RBC. We also investigate the temporal dynamics of an RBC membrane in real time. Temporal fluctuations associated with the selected points A, B, and C, respectively, on the RBC, central region of the RBC, and background region outside the RBC are plotted in Figs. 4(c) and 4(e). The corresponding SDs (σ) of fluctuations are computed as $\sigma_A = 67.8 \text{ nm}$, $\sigma_B = 39.4 \text{ nm}$, and

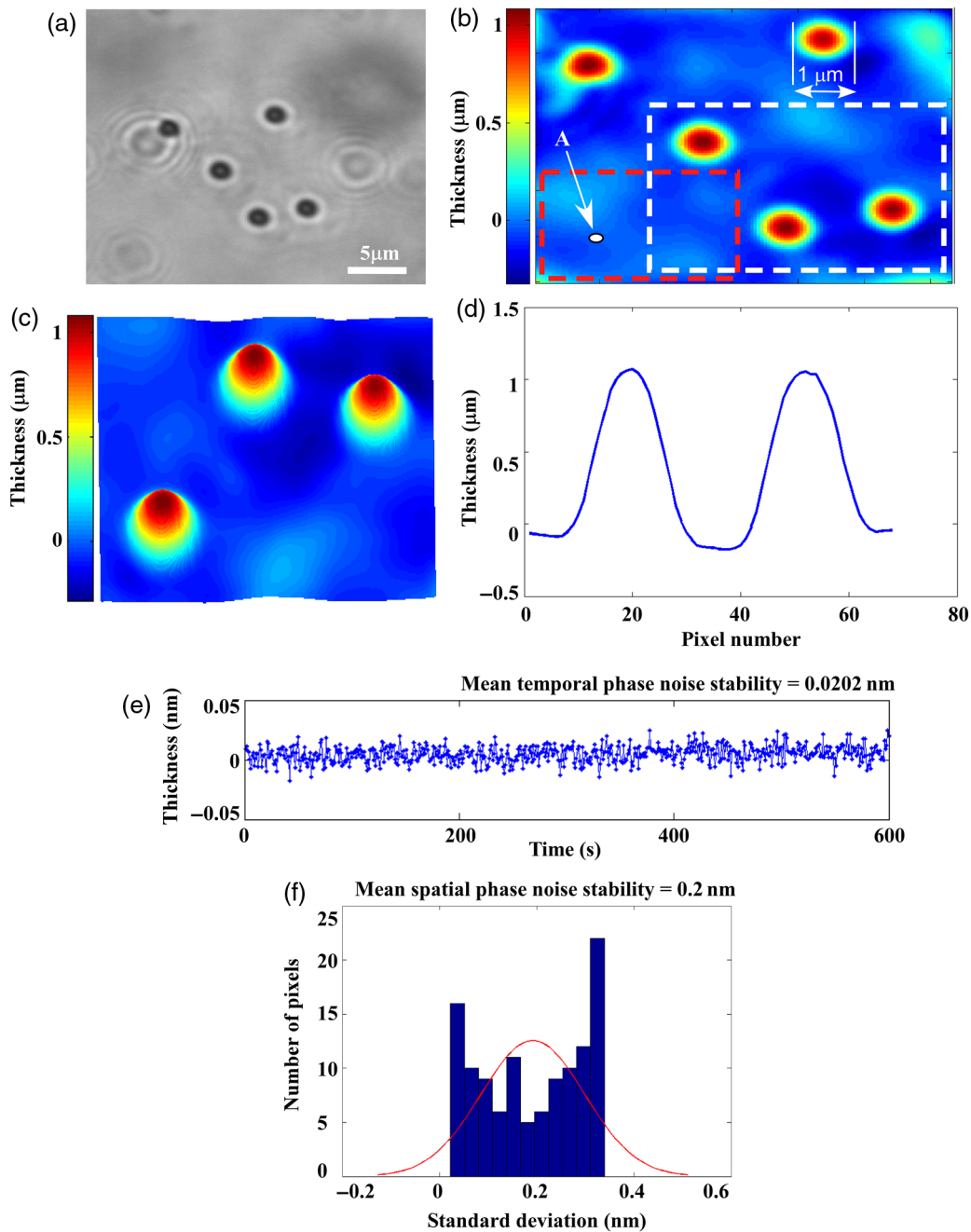


Fig. 2 Reconstructed 3-D images using single defocused TIE imaging. (a) Recorded bright-field defocused image with a defocus distance of $1 \mu\text{m}$, (b) reconstructed phase image, (c) 3-D view of the microbeads from the shown white color marked region in (b), and (d) profile of the microbeads showing its thickness. (e) Mean SD of temporal spatial noise for the point A in (b) is measured to be 0.02 nm . (f) Mean spatial noise SD for the 50×50 pixel region shown in red color (b) is 0.2 nm .

$\sigma_C = 9.6 \text{ nm}$, respectively. A video depicting the dynamics of RBC membrane fluctuations is illustrated in the file (Video 1, MPEG, 6.44 MB).

From our first observations, the results accurately render the 3-D structure and morphology of RBCs as reported in the literature. There is a strong contrast outlining the outer surface boundaries in all images (commonly called halos).⁵³ This is because, in the near-field regime and at intermediate distances between the sample and detector, self-interference patterns resulting in “Fresnel fringes” are formed under partially coherent illumination. In contrast to coherent interferometry, the recorded

intensity patterns are not proportional to the phase itself, but to the second derivative (the Laplacian) of the phase of the wave front. Therefore, the reconstruction method is most sensitive to abrupt changes in the decrement of the refractive index. This leads to strong halos surrounding the boundaries of the images. This approach also suffers from amplified noise for low spatial frequencies, thus slowly varying components may not be accurately recovered.⁵³ These effects or drawbacks are well known for systems using partially coherent light. The noise stability is another factor that affects the background thickness with respect to focal drift.^{54,55}

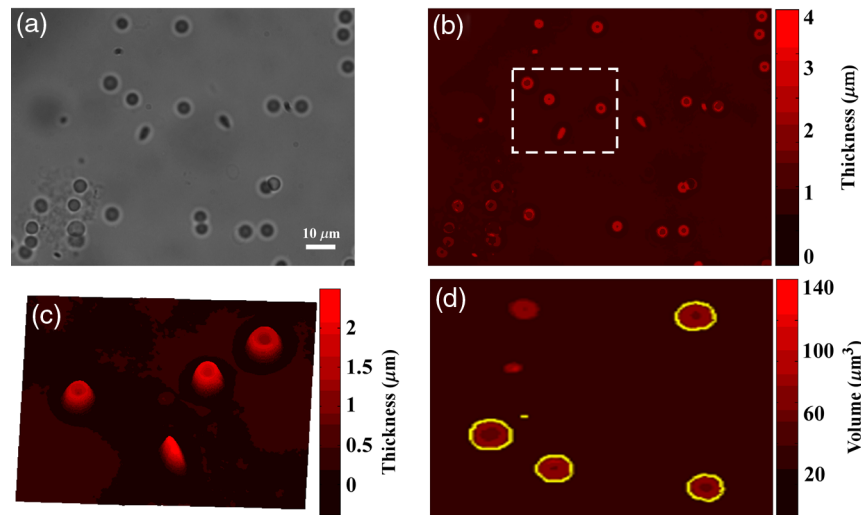


Fig. 3 Reconstructed 3-D images using single defocused TIE imaging. (a) Recorded bright-field defocused image with a defocus distance of $15\ \mu\text{m}$, (b) reconstructed phase image, (c) 3-D view of the RBCs from the marked region in (b), and (d) average volume of RBCs.

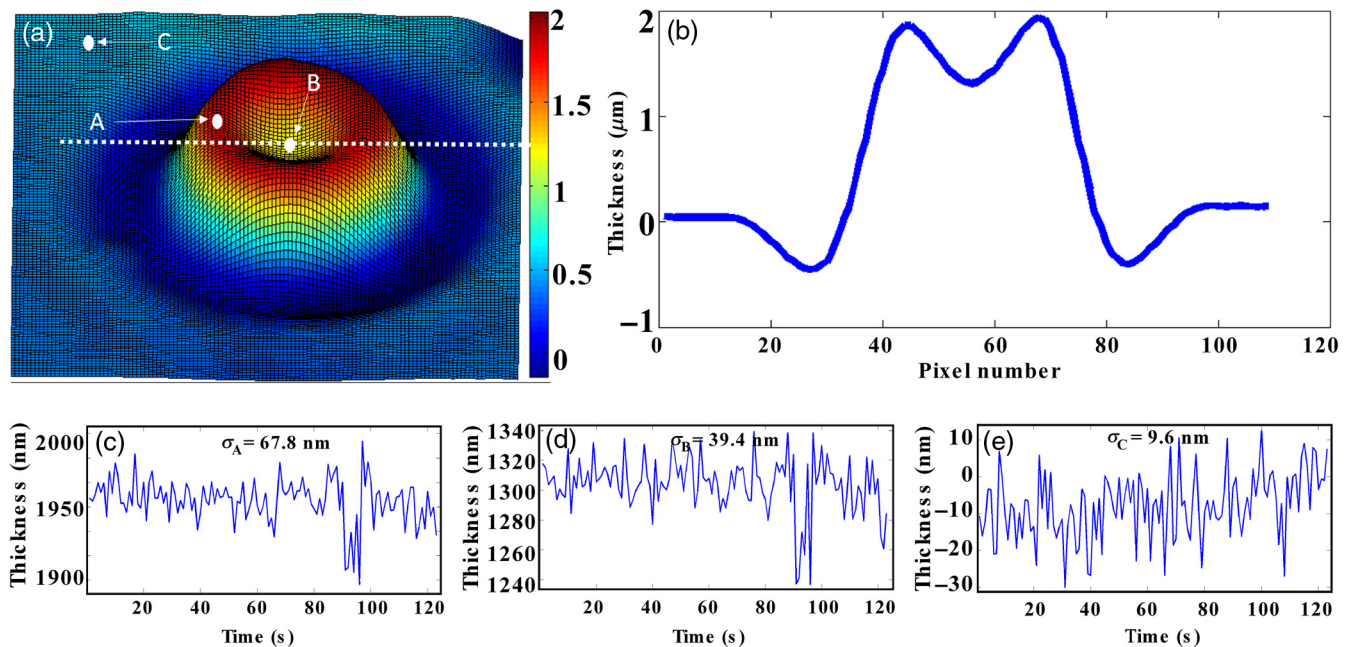


Fig. 4 Real-time dynamics of RBC membrane from 3-D images: (a) 3-D reconstructed image and (b) line profile depicting the accurate characteristic structure of RBC across the line shown in (a). (c)–(e) Nanometric membrane fluctuations on points A, B, and C, respectively. SDs of the fluctuations are $\sigma_A = 67.8\ \text{nm}$ (at point A on RBC membrane), $\sigma_B = 39.4\ \text{nm}$ (middle region of the RBC), and $\sigma_C = 9.6\ \text{nm}$ (background outside RBC). Real-time video of membrane fluctuations of the RBC (Video 1, MPEG, 6.44 MB [URL: <http://dx.doi.org/10.1117/1.JBO.22.10.106001.1>]).

This technique is identical to the conventional TIE principle except for one condition, i.e., only one defocused bright-field image is needed for quantitative phase reconstruction instead of three axially defocused bright-field images^{29–31} as the algorithm assumes the object to be homogenous with a known linear attenuation coefficient. This condition makes the experiment analogous to an inline holography setup, where the defocused image can be treated as a self-interferogram.³⁹ The main advantage of this technique is that we can directly calculate the thickness with the help of a single defocused image. Lambert–Beer’s

law $\{I = I_0 \exp[-\mu t(r_{\perp}, z)]\}$ has been substituted in place of the in-focus image intensity. Hence, from Eq. (9), the final thickness would depend on μ , the attenuation coefficient (absorption in liquid samples). Equation (9) was originally derived based on the assumption that (a) the incident beam is a monochromatic plane beam (or with mild curvature) with near-field conditions and (b) the object is single monomorphous (homogenous material). However, previous reports using polychromatic, low-coherence x-rays have explicitly mentioned that the theory and the equation are applicable over a wide parameter range and

in particular for polychromatic beams, on objects with low-density variations, and for objects with very weak absorption coefficients.⁵⁶ Considering the denominator term in Eq. (9) $R_2 \Delta n |k_\perp|^2 + \mu$, the first additive term corresponds to phase contrast, and the second term corresponds to absorption contrast. It is easy to verify that the phase contrast term is dominant at all nonzero spatial frequencies, as absorption has been assumed to be weak. From the above denominator term in Eq. (9), it is true that this technique will work for weakly absorbing biological samples.

Concerning the spectral dependence of the absorption coefficient, especially in the case of RBCs reported here, the absorption coefficient changes from 0.1 to 0.3 μm^{-1} in the spectral range that we are considering (450 to 600 nm). Assuming a weak absorption coefficient, our logic of using the absorption coefficient of the central wavelength can be justified for simplicity reasons.

Another way to arrive at an effective absorption coefficient has been proposed by Arhatari et al.,^{57,58} for polychromatic x-rays based on the equation given below.

The effective absorption coefficient for a polychromatic beam can be obtained as

$$\mu_{\text{eff}} = \frac{\int \mu_\lambda I_\lambda^{\text{in}}(r) D(\lambda) d\lambda}{\int I_\lambda^{\text{in}}(r) D(\lambda) d\lambda}, \quad (10)$$

where $I_\lambda^{\text{in}}(r)$ is the intensity entering the sample, μ_λ the monochromatic values for μ , and $D(\lambda)$ is the combined detector response and optical path length. The denominator is the polychromatic incident intensity $I_{\text{poly}}^{\text{in}}(r)$. In fact, there has been an independent effort from Zysk et al.⁵⁹ to treat TIE as the transport of spectra intensities and accurately calculate phase for each coherent mode. This would need multiple spectral measurements to arrive at the phases of each coherent mode. Phase retrieval from a single defocused image using the TIE technique can essentially be considered as a combination of common-path geometry with single-shot capability, allowing fast and stable quantitative phase imaging. In summary, the results reported in this paper show the high potential of TIEM as a fast screening tool for real-time 3-D volumetric imaging and quantification of enucleated biological cells such as RBCs.

5 Conclusions

We have demonstrated quantitative phase reconstruction of live RBCs using the TIE principle from a single defocused image. The main assumption in this experiment is that the sample is homogenous. Hence, this technique will be highly accurate for homogenous cells like RBCs. We believe that the technique will serve as a powerful tool for noncontact characterization of RBCs in studying their structural morphology and RBC membrane fluctuations. The main advantage of this technique is that no sophisticated experimental setups are needed in realizing this reconstruction since a conventional bright-field microscope can deliver defocused images of the sample. This technique will facilitate high throughput screening and analysis of structural and morphological properties of RBCs, which will be highly useful in screening for diseases such as sickle cell anemia and malarial infections.

Appendix

The identity [Eq. (5)] is

$$\Delta n \nabla_\perp \cdot [e^{-\mu t(r_\perp, z)} \nabla_\perp t(r_\perp, z)] = -\frac{\Delta n}{\mu} \nabla_\perp^2 e^{-\mu t(r_\perp, z)}.$$

We take right-hand side and derive left-hand side (LHS) to prove the above identity

$$\Rightarrow -\frac{\Delta n}{\mu} \nabla_\perp^2 e^{-\mu t(r_\perp, z)}.$$

Using the Laplacian identity $\nabla^2 f = \nabla \cdot \nabla f = \text{div grad } f$

$$\begin{aligned} \Rightarrow & -\frac{\Delta n}{\mu} \nabla_\perp \cdot \left[\nabla_\perp e^{-\mu t(r_\perp, z)} \right], \\ \Rightarrow & -\frac{\Delta n}{\mu} \nabla_\perp \cdot \{ -\mu e^{-\mu t(r_\perp, z)} \nabla_\perp [t(r_\perp, z)] \}, \\ \Rightarrow & \Delta n \nabla_\perp \cdot [e^{-\mu t(r_\perp, z)} \nabla_\perp t(r_\perp, z)], \end{aligned}$$

which is equal to LHS.

Disclosures

The authors have no relevant financial interests in this article and no potential conflicts of interest to disclose.

Acknowledgments

The authors acknowledge Shanti Diagnostics, Hyderabad, for providing RBC samples. One of the authors, Dr. Renu John, acknowledges financial support from the Science and Engineering Research Board (SERB), DST, India (No. SR/S2/LOP-0024/2012) and BRNS, India (No. 34/14/04/2015/BRNS).

References

1. F. Zernike, "Phase contrast, a new method for the microscopic observation of transparent objects," *Physica* **9**(7), 686–698 (1942).
2. H. E. Rosenberger, "Differential interference contrast microscopy," in *Interpretive Techniques for Microstructural Analysis*, pp. 79–104, Springer, Boston, Massachusetts (1977).
3. D. J. Stephens and V. J. Allan, "Light microscopy techniques for live cell imaging," *Science* **300**(5616), 82–86 (2003).
4. J. C. H. Spence, *Experimental High-Resolution Electron Microscopy*, Oxford University Press, Oxford, United Kingdom (1988).
5. X. Michalet et al., "Quantum dots for live cells, in vivo imaging, and diagnostics," *Science* **307**(5709), 538–544 (2005).
6. Y. Urano et al., "Selective molecular imaging of viable cancer cells with pH-activatable fluorescence probes," *Nat. Med.* **15**(1), 104–109 (2009).
7. P. Marquet et al., "Digital holographic microscopy: a noninvasive contrast imaging technique allowing quantitative visualization of living cells with subwavelength axial accuracy," *Opt. Lett.* **30**(5), 468–470 (2005).
8. M. K. Kim, *Digital Holographic Microscopy*, Springer, New York (2011).
9. G. Popescu, *Quantitative Phase Imaging of Cells and Tissues*, McGraw Hill Professional, New York (2011).
10. G. Popescu, "Quantitative phase imaging of nanoscale cell structure and dynamics," *Methods Cell Biol.* **90**, 87–115 (2008).
11. U. Schnars and W. P. O. Jüptner, "Digital recording and numerical reconstruction of holograms," *Meas. Sci. Tech.* **13**(9), R85 (2002).
12. G. Popescu et al., "Fourier phase microscopy for investigation of biological structures and dynamics," *Opt. Lett.* **29**(21), 2503–2505 (2004).
13. G. Popescu, R. R. Dasari, and M. S. Feld, "Hilbert phase microscopy for investigating fast dynamics in transparent systems," *Opt. Lett.* **30**(10), 1165–1167 (2005).

14. G. Popescu et al., "Diffraction phase microscopy for quantifying cell structure and dynamics," *Opt. Lett.* **31**(6), 775–777 (2006).
15. E. Cuche, P. Marquet, and C. Depeursinge, "Simultaneous amplitude-contrast and quantitative phase-contrast microscopy by numerical reconstruction of Fresnel off-axis holograms," *Appl. Opt.* **38**(34), 6994–7001 (1999).
16. V. P. Pandiyan, K. Khare, and R. John, "Quantitative phase imaging of live cells with near on-axis digital holographic microscopy using constrained optimization approach," *J. Biomed. Opt.* **21**(10), 106003 (2016).
17. V. P. Pandiyan and R. John, "Optofluidic bioimaging platform for quantitative phase imaging of lab on a chip devices using digital holographic microscopy," *Appl. Opt.* **55**(3), A54–A59 (2016).
18. J. Garcia-Sucerquia et al., "Digital in-line holographic microscopy," *Appl. Opt.* **45**(5), 836–850 (2006).
19. W. Choi et al., "Tomographic phase microscopy," *Nat. Methods* **4**(9), 717–719 (2007).
20. Z. Wang et al., "Spatial light interference microscopy (SLIM)," *Opt. Express* **19**(2), 1016–1026 (2011).
21. N. T. Shaked et al., "Quantitative microscopy and nanoscopy of sickle red blood cells performed by wide field digital interferometry," *J. Biomed. Opt.* **16**(3), 030506 (2011).
22. S. K. Debnath and Y. K. Park, "Real-time quantitative phase imaging with a spatial phase-shifting algorithm," *Opt. Lett.* **36**(23), 4677–4679 (2011).
23. Y. K. Park et al., "Spectroscopic phase microscopy for quantifying hemoglobin concentrations in intact red blood cells," *Opt. Lett.* **34**(23), 3668–3670 (2009).
24. H. Pham et al., "Spectroscopic diffraction phase microscopy," *Opt. Lett.* **37**(16), 3438–3440 (2012).
25. D. Fu et al., "Quantitative dispersion microscopy," *Biomed. Opt. Express* **1**(2), 347–353 (2010).
26. M. Rinehart, Y. Zhu, and A. Wax, "Quantitative phase spectroscopy," *Biomed. Opt. Express* **3**(5), 958–965 (2012).
27. Y. Jang, J. Jang, and Y. K. Park, "Dynamic spectroscopic phase microscopy for quantifying hemoglobin concentration and dynamic membrane fluctuation in red blood cells," *Opt. Express* **20**(9), 9673–9681 (2012).
28. A. Sagisaka et al., "Development of a two-color interferometer for observing wide range electron density profiles with a femtosecond time resolution," *Appl. Phys. B* **84**(3), 415–419 (2006).
29. A. Barty et al., "Quantitative optical phase microscopy," *Opt. Lett.* **23**(11), 817–819 (1998).
30. N. Streibl, "Phase imaging by the transport equation of intensity," *Opt. Commun.* **49**(1), 6–10 (1984).
31. P. K. Poola, V. P. Pandiyan, and R. John, "Non-interferometric quantitative phase imaging of yeast cells," *Proc. SPIE* **9792**, 97920G (2015).
32. D. Paganin and K. A. Nugent, "Noninterferometric phase imaging with partially coherent light," *Phys. Rev. Lett.* **80**(12), 2586–2589 (1998).
33. L. Waller et al., "Phase from chromatic aberrations," *Opt. Express* **18**(22), 22817–22825 (2010).
34. S. S. Gorthi and E. Schonbrun, "Phase imaging flow cytometry using a focus-stack collecting microscope," *Opt. Lett.* **37**(4), 707–709 (2012).
35. L. Waller et al., "Transport of intensity phase imaging in a volume holographic microscope," *Opt. Lett.* **35**(17), 2961–2963 (2010).
36. C. Zuo et al., "Noninterferometric single-shot quantitative phase microscopy," *Opt. Lett.* **38**(18), 3538–3541 (2013).
37. C. Zuo et al., "High-speed transport-of-intensity phase microscopy with an electrically tunable lens," *Opt. Express* **21**(20), 24060–24075 (2013).
38. L. Camacho et al., "Quantitative phase microscopy using defocusing by means of a spatial light modulator," *Opt. Express* **18**(7), 6755–6766 (2010).
39. D. Paganin et al., "Simultaneous phase and amplitude extraction from a single defocused image of a homogeneous object," *J. Microsc.* **206**(1), 33–40 (2002).
40. T. E. Gureyev et al., "Linear algorithms for phase retrieval in the Fresnel region," *Opt. Commun.* **231**(1), 53–70 (2004).
41. D. Paganin and K. A. Nugent, *Advances in Imaging and Electron Physics*, Vol. **118**, P. Hawkes, Ed., pp. 85–127, Harcourt Publishers, Kent (2001).
42. G. Popescu et al., "Imaging red blood cell dynamics by quantitative phase microscopy," *Blood Cells, Mol. Dis.* **41**(1), 10–16 (2008).
43. G. Popescu et al., "Erythrocyte structure and dynamics quantified by Hilbert phase microscopy," *J. Biomed. Opt.* **10**(6), 060503 (2005).
44. G. Popescu et al., "Observation of dynamic subdomains in red blood cells," *J. Biomed. Opt.* **11**(4), 040503 (2006).
45. U. Agero et al., "Cell surface fluctuations studied with defocusing microscopy," *Phys. Rev. E* **67**(5), 051904 (2003).
46. U. Agero et al., "Defocusing microscopy," *Microsc. Res. Tech.* **65**(3), 159–165 (2004).
47. L. G. Mesquita, U. Agero, and O. N. Mesquita, "Defocusing microscopy: an approach for red blood cell optics," *Appl. Phys. Lett.* **88**(13), 133901 (2006).
48. G. Popescu et al., "Optical measurement of cell membrane tension," *Phys. Rev. Lett.* **97**(21), 218101 (2006).
49. S. Wang et al., "Phase retrieval method for biological samples with absorption," *J. Opt.* **15**(7), 075301 (2013).
50. O. Zernovaya et al., "The refractive index of human hemoglobin in the visible range," *Phys. Med. Biol.* **56**(13), 4013–4021 (2011).
51. M. L. Turgeon, *Clinical Hematology: Theory and Procedures*, Lippincott Williams & Wilkins, Philadelphia (2005).
52. C. E. McLaren, G.M. Brittenham, and V. I. C. T. O. R. Hasselblad, "Statistical and graphical evaluation of erythrocyte volume distributions," *Am. J. Physiol. Heart. Circ. Physiol.* **252**(4), H857–H866 (1987).
53. T. H. Nguyen et al., "Halo-free phase contrast microscopy," *Sci. Rep.* **7**, 44034 (2017).
54. L. Waller, L. Tian, and G. Barbastathis, "Transport of intensity phase-amplitude imaging with higher order intensity derivatives," *Opt. Express*, **18**(12), 12552–12561 (2010).
55. D. Paganin et al., "Quantitative phase-amplitude microscopy. III. The effects of noise," *J. Microsc.* **214**(1), 51–61 (2004).
56. T. Weitkamp et al., "ANKAphase: software for single-distance phase retrieval from inline x-ray phase-contrast radiographs," *J. Synchrotron Radiat.* **18**(4), 617–629 (2011).
57. B. D. Arhatari et al., "Phase imaging using a polychromatic x-ray laboratory source," *Opt. Express* **16**(24), 19950–19956 (2008).
58. B. D. Arhatari, G. van Riessen, and A. Peele, "Polychromatic x-ray tomography: direct quantitative phase reconstruction," *Opt. Express* **20**(21), 23361–23366 (2012).
59. A. M. Zysk et al., "Transport of intensity and spectrum for partially coherent fields," *Opt. Lett.* **35**, 2239–2241 (2010).

Praveen Kumar Poola received his BTech degree from Kakatiya University, Warangal, India, in 2010 with electronics and instrumentation specialization, and his master's of design degree from the Indian Institute of Information Technology Design and Manufacturing, Kancheeppuram, India, in 2013 with electronic systems design specialization. He is currently pursuing his PhD in biomedical engineering at the Indian Institute of Technology Hyderabad. His current research interests include low-coherence optical imaging applications and the development of algorithms for noninterferometric phase imaging.

Renu John received his PhD from the Indian Institute of Technology Delhi in 2006. He carried out his postdoctoral research at Fitzpatrick Center for Photonics, Duke University, Durham, North Carolina, and Biophotonics Imaging Laboratory, University of Illinois, Urbana-Champaign. He is currently an associate professor and head of the Department of Biomedical Engineering at the Indian Institute of Technology Hyderabad. His research interests include nanobiophotonics, noninvasive NIR bioimaging, three-dimensional phase microscopy, and optical coherence tomography.